

Lensing contribution to the 21cm intensity bispectrum

Rahul Kothari,^a Roy Maartens^{a,b}

^aDepartment of Physics and Astronomy, University of the Western Cape, South Africa

^bInstitute of Cosmology & Gravitation, University of Portsmouth, Portsmouth PO1 3FX, UK

E-mail: quantummechanickothari@gmail.com, roy.maartens@gmail.com

Abstract. Intensity maps of the 21cm emission line of neutral hydrogen are lensed by intervening large-scale structure, similar to the lensing of the cosmic microwave background temperature map. We extend previous work by calculating the lensing contribution to the full-sky 21cm bispectrum in redshift space. The lensing contribution tends to peak when equal-redshift fluctuations are lensed by a lower redshift fluctuation. At high redshift, lensing effects can become comparable to the contributions from density and redshift-space distortions.

1 Introduction

The cosmic microwave background (CMB) has been an invaluable probe for developing and testing cosmological models. Its main constraining power comes from the primary anisotropies that are imprinted at $z \sim 1000$. In addition to this, it also contributes to low-redshift constraints via the lensing of the CMB temperature by large-scale structure [1]. The integrated 21cm emission from neutral hydrogen (HI) in the post-reionisation era produces maps that are qualitatively similar to the CMB, but with multiple maps over a range of redshifts. 21cm intensity maps are also lensed by intervening large-scale structure. For surveys that detect individual galaxies, the lensing effect on number density occurs at first order in perturbations and modifies the tree-level power spectrum. In the case of the CMB and 21cm intensity mapping, the first-order lensing effect vanishes due to conservation of surface brightness [2, 3]: the lensing effect in the CMB and 21cm intensity arises at second order. As a result, the 21cm power spectrum is only affected at 1-loop level [4, 5]. By contrast, the tree-level 21cm bispectrum does carry an imprint of lensing, as pointed out in [5–7].

In this paper, our aim is to derive the lensing contribution to the 21cm angular bispectrum and present some numerical examples. The result includes redshift-space distortions (RSD). Since we work in angular harmonic space, wide-angle correlations are naturally included, i.e., there is no flat-sky approximation.

The HI temperature contrast observed in redshift space is denoted $\Delta \equiv \Delta_{\text{HI}} = \Delta T_{\text{HI}} / \langle T_{\text{HI}} \rangle$. The lensed temperature contrast at redshift z and in direction \mathbf{n} is related to the unlensed one as

$$\Delta^{\text{L}}(z, \mathbf{n}) = \Delta(z, \mathbf{n} + \nabla_{\perp} \phi(z, \mathbf{n})), \quad (1.1)$$

where ∇_{\perp} is the gradient operator on the 2-sphere orthogonal to \mathbf{n} , and ϕ is the lensing potential. At first order (which is all that is needed for the tree-level bispectrum),

$$\phi^{(1)} = - \int_0^r d\tilde{r} \frac{(r - \tilde{r})}{r\tilde{r}} \left[\Phi^{(1)} + \Psi^{(1)} \right], \quad (1.2)$$

where r is the comoving line-of-sight distance and the metric potentials in Poisson gauge are given by (neglecting vector and tensor modes)

$$ds^2 = a^2 \left[- (1 + 2\Psi) d\eta^2 + (1 - 2\Phi) d\mathbf{x}^2 \right]. \quad (1.3)$$

At first order, (1.1) implies that $\Delta^{\text{L}(1)} = \Delta^{(1)}$, so that up to second order we have

$$\Delta^{\text{L}}(z, \mathbf{n}) = \Delta^{(1)}(z, \mathbf{n}) + \Delta^{(2)}(z, \mathbf{n}) - \langle \Delta^{(2)} \rangle(z) + L^{(2)}(z, \mathbf{n}) - \langle L^{(2)} \rangle(z), \quad (1.4)$$

where our convention is $\Delta = \Delta^{(1)} + \Delta^{(2)}$ and we have subtracted averages in order to ensure that $\langle \Delta^{\text{L}}(z, \mathbf{n}) \rangle = 0$. The unlensed temperature contrasts are [4–6]

$$\Delta^{(1)} = b_1 \delta^{(1)} + \frac{1}{\mathcal{H}} \partial_r^2 V^{(1)}, \quad (1.5)$$

$$\begin{aligned} \Delta^{(2)} = & b_1 \delta^{(2)} + \frac{1}{2} b_2 [\delta^{(1)}]^2 + b_s s^2 \\ & + \frac{1}{\mathcal{H}} \partial_r^2 V^{(2)} + \frac{1}{\mathcal{H}^2} \left([\partial_r^2 V^{(1)}]^2 + \partial_r V^{(1)} \partial_r^3 V^{(1)} \right) + \frac{1}{\mathcal{H}} \left[\partial_r V^{(1)} \partial_r \delta^{(1)} + \delta^{(1)} \partial_r^2 V^{(1)} \right], \end{aligned} \quad (1.6)$$

where δ is the matter density contrast, $\partial_r = \mathbf{n} \cdot \nabla$ and the velocity potential is defined so that the peculiar velocity is $\mathbf{v} = \nabla V$. Terms with radial gradients of V constitute the

RSD contribution. The linear and quadratic clustering bias parameters are assumed scale-independent, i.e., $b_i = b_i(z)$. The tidal contribution to clustering bias has bias parameter $b_s(z)$ multiplying $s^2 = s_{ij}s^{ij}$, where the tidal field is

$$s_{ij} = \left(\partial_i \partial_j - \frac{1}{3} \delta_{ij} \nabla^2 \right) \nabla^{-2} \delta^{(1)}. \quad (1.7)$$

In the case of galaxy surveys, the lensing contribution to number count fluctuations at first and second orders includes the lensing convergence,

$$\kappa = -\frac{1}{2} \nabla_{\perp a} \nabla_{\perp}^a \phi. \quad (1.8)$$

By contrast, lensing of HI intensity fluctuations at leading order (i.e. second order) does *not* include the lensing convergence. Instead, it is given purely by a coupling of the lensing deflection angle $\nabla_{\perp}^a \phi$ with the screen-space gradient of the observed temperature contrast $\nabla_{\perp a} \Delta$ [4, 6]:

$$L^{(2)}(z, \mathbf{n}) = \nabla_{\perp}^a \phi^{(1)}(z, \mathbf{n}) \nabla_{\perp a} \Delta^{(1)}(z, \mathbf{n}). \quad (1.9)$$

The same form of lensing contribution arises in the CMB. However, in the CMB case, the coupling in (1.9) is negligible, since there is effectively no correlation between primary CMB temperature fluctuations $\nabla_{\perp a} \Delta_{\text{cmb}}^{(1)}$, that are generated at $z \sim 1000$, and the lensing deflections $\nabla_{\perp}^a \phi^{(1)}$, that are induced by the large-scale structure at low z [5] (see the review [8] for further details). This correlation is not negligible for post-reionisation 21cm intensity mapping, since the fluctuations $\nabla_{\perp a} \Delta^{(1)}$ are growing after reionisation, i.e., at $z \lesssim 6$, where lensing deflections from large-scale structure are also growing. (For further details on the cosmological evolution of 21cm intensity fluctuations from recombination through reionisation to the present time, see e.g. the review [9].) Thus we expect that the lensing contribution to the bispectrum is nonzero at tree level.

The full-sky redshift-space bispectrum based on (1.4)–(1.6) has not been previously presented, as far as we are aware. A partial result was given in [6], where HI clustering bias and RSD were neglected in the lensing contribution. In [7], the redshift-space bispectrum with HI clustering bias was presented, but the lensing contribution was omitted.

The article is structured as follows. In Section 2, we derive the expression of the lensing contribution to the bispectrum in redshift space. We show that the lensing contribution is typically much smaller than the unlensed bispectrum. However, it can become significant when high-redshift correlations are lensed by a lower redshift fluctuation. We conclude in Section 3. In Appendix B, we present the lensing contribution to the 21cm intensity 4-point correlation function, which is relevant for the variance of the lensed HI intensity mapping power spectrum.

In this article, we consider a fiducial flat Λ CDM cosmology with dimensionless Hubble constant $h = 0.67$, baryon and cold dark matter density parameters $\Omega_b = 0.05$ and $\Omega_{\text{cdm}} = 0.27$, primordial scalar amplitude and tilt $A_s = 2.3 \times 10^{-9}$ and $n_s = 0.962$, evaluated at pivot scale $k_* = 0.05 \text{ Mpc}^{-1}$.

2 Lensed bispectrum

The lensed 3-point correlation function is

$$\begin{aligned} B^{\text{L}}(z_1, \mathbf{n}_1, z_2, \mathbf{n}_2, z_3, \mathbf{n}_3) &= \langle \Delta_1^{\text{L}} \Delta_2^{\text{L}} \Delta_3^{\text{L}} \rangle \quad \text{where} \quad \Delta_i \equiv \Delta(z_i, \mathbf{n}_i) \\ &= \langle \Delta_1 \Delta_2 \Delta_3 \rangle + \delta B(z_1, \mathbf{n}_1, z_2, \mathbf{n}_2, z_3, \mathbf{n}_3). \end{aligned} \quad (2.1)$$

At tree level, the lensing correction is

$$\delta B(z_i, \mathbf{n}_i) = \left\langle \Delta_1^{(1)} \Delta_2^{(1)} \left[L_3^{(2)} - \langle L_3^{(2)} \rangle \right] \right\rangle + 2 \text{ perms.} \quad (2.2)$$

Using (1.9) in (2.2) and applying Wick's theorem, we find that

$$\delta B(z_i, \mathbf{n}_i) = \langle \Delta_1^{(1)} \nabla_\perp^a \phi_3 \rangle \langle \Delta_2^{(1)} \nabla_{\perp a} \Delta_3^{(1)} \rangle + \langle \Delta_2^{(1)} \nabla_\perp^a \phi_3 \rangle \langle \Delta_1^{(1)} \nabla_{\perp a} \Delta_3^{(1)} \rangle + 2 \text{ perms.} \quad (2.3)$$

The corresponding lensing correction to the angular bispectrum is given by

$$\delta B(z_i, \mathbf{n}_i) = \sum_{\ell_i m_i} \delta B_{\ell_1 \ell_2 \ell_3}^{m_1 m_2 m_3}(z_1, z_2, z_3) Y_{\ell_1 m_1}(\mathbf{n}_1) Y_{\ell_2 m_2}(\mathbf{n}_2) Y_{\ell_3 m_3}(\mathbf{n}_3). \quad (2.4)$$

We now derive the expression for $\delta B_{\ell_1 \ell_2 \ell_3}^{m_1 m_2 m_3}(z_1, z_2, z_3)$, starting with the first term of (2.3):

$$\begin{aligned} \langle \Delta_1^{(1)} \nabla_\perp^a \phi_3 \rangle \langle \Delta_2^{(1)} \nabla_{\perp a} \Delta_3^{(1)} \rangle &= \sum \langle \Delta_{\ell_1 m_1}(z_1) \phi_{\ell_3 m_3}(z_3) \rangle \langle \Delta_{\ell_2 m_2}(z_2) \Delta_{\ell_4 m_4}(z_3) \rangle \\ &\quad \times Y_{\ell_1 m_1}(\mathbf{n}_1) Y_{\ell_2 m_2}(\mathbf{n}_2) \nabla_\perp^a Y_{\ell_3 m_3}(\mathbf{n}_3) \nabla_{\perp a} Y_{\ell_4 m_4}(\mathbf{n}_3). \end{aligned} \quad (2.5)$$

The harmonic expansion of gradients of the spherical harmonics can be computed using spin spherical harmonics and the lowering and raising operators [6] (see Appendix A for further details). This leads to

$$\begin{aligned} \nabla_\perp^a Y_{\ell_3 m_3}(\mathbf{n}) \nabla_{\perp a} Y_{\ell_4 m_4}(\mathbf{n}) &= -\frac{1}{2} \sqrt{\ell_3 \ell_4 (\ell_3 + 1)(\ell_4 + 1)} \sum_{\ell m} (-1)^m Y_{\ell m}(\mathbf{n}) \left[1 + (-1)^{\ell_3 + \ell_4 + \ell} \right] \\ &\quad \times \sqrt{\frac{(2\ell + 1)(2\ell_3 + 1)(2\ell_4 + 1)}{4\pi}} \begin{pmatrix} \ell_3 & \ell_4 & \ell \\ m_3 & m_4 & -m \end{pmatrix} \begin{pmatrix} \ell_3 & \ell_4 & \ell \\ 1 & -1 & 0 \end{pmatrix}, \end{aligned} \quad (2.6)$$

where the 3×2 matrices are Wigner 3j symbols (evaluated with the `wigxjpf` code [10]). The second term of (2.3) follows similarly.

Using (2.5) and (2.6), together with their counterparts for the second term of (2.3), we find that the lensing contribution to the angular bispectrum is

$$\begin{aligned} \delta B_{\ell_1 \ell_2 \ell_3}^{m_1 m_2 m_3} &= - \left[C_{\ell_1}^{\Delta\Delta}(z_1, z_3) C_{\ell_2}^{\Delta\phi}(z_2, z_3) + C_{\ell_1}^{\Delta\phi}(z_1, z_3) C_{\ell_2}^{\Delta\Delta}(z_2, z_3) \right] \begin{pmatrix} \ell_1 & \ell_2 & \ell_3 \\ 1 & -1 & 0 \end{pmatrix} \begin{pmatrix} \ell_1 & \ell_2 & \ell_3 \\ m_1 & m_2 & m_3 \end{pmatrix} \\ &\quad \times \sqrt{\frac{\ell_1 \ell_2 (\ell_1 + 1)(\ell_2 + 1)(2\ell_1 + 1)(2\ell_2 + 1)(2\ell_3 + 1)}{4\pi}} + 2 \text{ perms.} \end{aligned} \quad (2.7)$$

Here the first-order angular power spectra C_ℓ^{XY} are defined by

$$\langle X_{\ell m}(z) Y_{\ell' m'}(z') \rangle = (-1)^m C_\ell^{XY}(z, z') \delta_{\ell \ell'} \delta_{m, -m'}, \quad (2.8)$$

where Δ denotes $\Delta_{\text{HI}}^{(1)}$ and ϕ denotes $\phi^{(1)}$, so that $C_\ell^{\Delta\Delta}$ is the HI intensity auto power spectrum and $C_\ell^{\Delta\phi}$ is the cross power spectrum of the lensing potential with HI intensity.

Statistical isotropy allows us to define the reduced lensing contribution to the bispectrum:

$$\delta B_{\ell_1 \ell_2 \ell_3}^{m_1 m_2 m_3}(z_1, z_2, z_3) = \mathcal{G}_{\ell_1 \ell_2 \ell_3}^{m_1 m_2 m_3} \delta b_{\ell_1 \ell_2 \ell_3}(z_1, z_2, z_3), \quad (2.9)$$

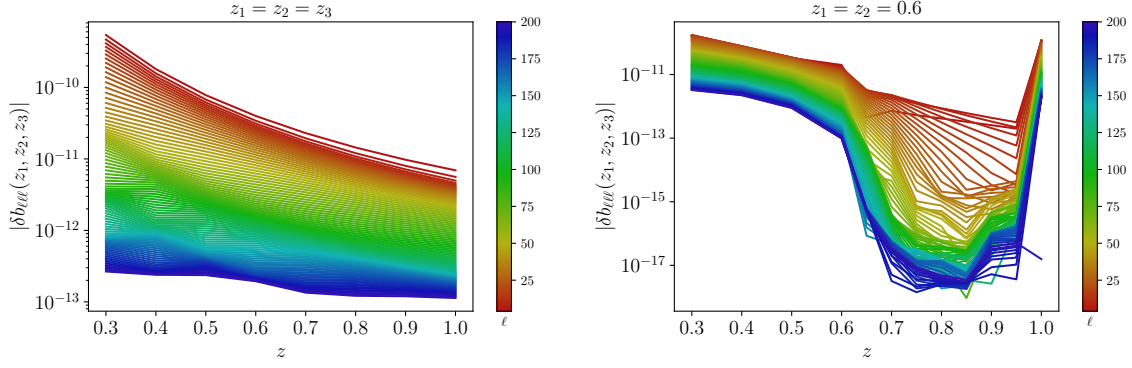


Figure 1. Lensing contribution $\delta b_{\ell\ell\ell}$ to the 21cm intensity bispectrum in the equilateral configuration, with three equal redshifts (left) and $z_1 = z_2 = 0.6$ fixed with varying z_3 (right). Colour bar shows the ℓ value.

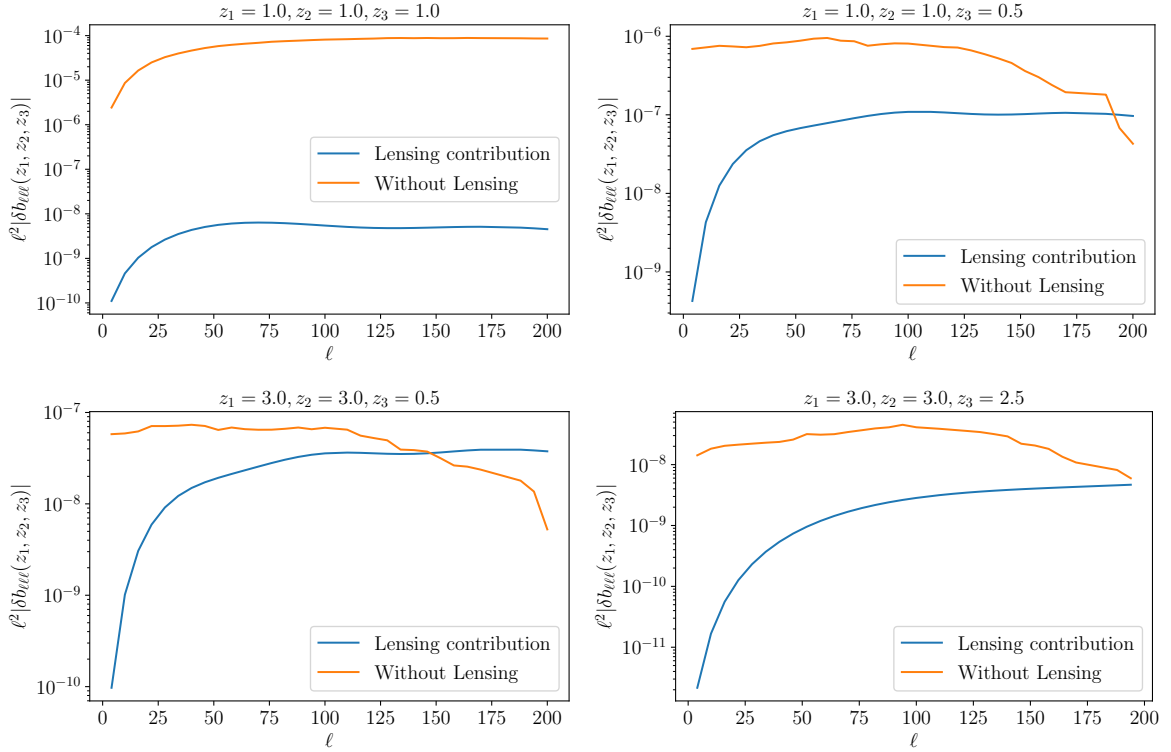


Figure 2. 21cm intensity mapping bispectrum in the equilateral configuration and for various redshift triples: without lensing ($b_{\ell\ell\ell}$, orange), lensing contribution ($\delta b_{\ell\ell\ell}$, blue).

where the Gaunt integral is

$$\mathcal{G}_{\ell_1\ell_2\ell_3}^{m_1m_2m_3} = \sqrt{\frac{(2\ell_1+1)(2\ell_2+1)(2\ell_3+1)}{4\pi}} \begin{pmatrix} \ell_1 & \ell_2 & \ell_3 \\ m_1 & m_2 & m_3 \end{pmatrix} \begin{pmatrix} \ell_1 & \ell_2 & \ell_3 \\ 0 & 0 & 0 \end{pmatrix}. \quad (2.10)$$

From (2.7) and (2.9), it follows that the lensing contribution to the reduced bispectrum is

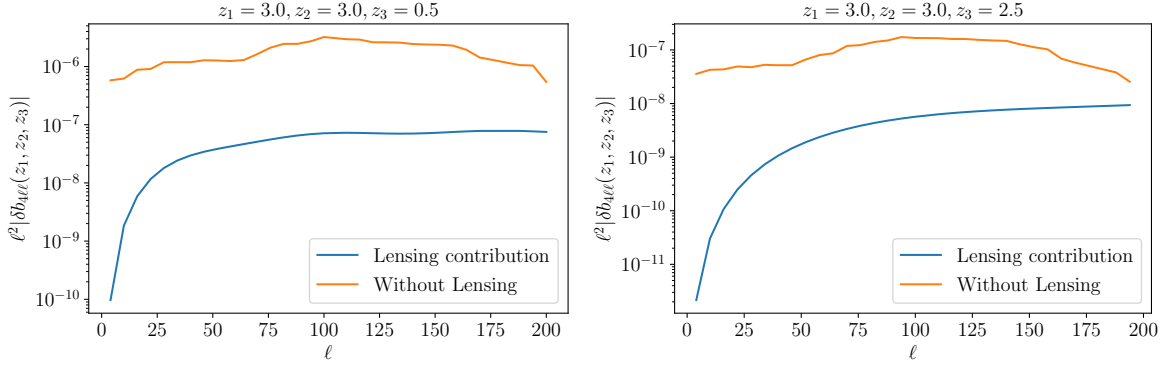


Figure 3. As in Figure 2, for isosceles configurations with $\ell_1 = 4, \ell_2 = \ell_3 \equiv \ell$. Squeezed configurations have $\ell \gg 4$.

given by

$$\begin{aligned} \delta b_{\ell_1 \ell_2 \ell_3} = & - \left[C_{\ell_1}^{\Delta\Delta}(z_1, z_3) C_{\ell_2}^{\Delta\phi}(z_2, z_3) + C_{\ell_1}^{\Delta\phi}(z_1, z_3) C_{\ell_2}^{\Delta\Delta}(z_2, z_3) \right] \\ & \times \begin{pmatrix} \ell_1 & \ell_2 & \ell_3 \\ 0 & 0 & 0 \end{pmatrix}^{-1} \begin{pmatrix} \ell_1 & \ell_2 & \ell_3 \\ 1 & -1 & 0 \end{pmatrix} \sqrt{\ell_1 \ell_2 (\ell_1 + 1)(\ell_2 + 1)} + 2 \text{ perms.} \end{aligned} \quad (2.11)$$

This is our main result. It extends the result of [7], which presented and computed the unlensed $b_{\ell_1 \ell_2 \ell_3}$ for 21cm intensity maps, and it recovers the special case in [6], where the RSD and clustering bias effects were neglected in $\delta b_{\ell_1 \ell_2 \ell_3}$.

Examples of the absolute value of the reduced bispectrum (2.11) are shown in Figures 1–3. We used CLASS [11, 12] for the lensed contribution $\delta b_{\ell_1 \ell_2 \ell_3}$ and the BYSPECTRUM code¹ [7, 13] for the unlensed bispectrum $b_{\ell_1 \ell_2 \ell_3}$. Following [7], we modelled the HI clustering bias parameters as

$$b_1(z) = 0.754 + 0.0877z + 0.0607z^2 - 0.00274z^3, \quad (2.12)$$

$$b_2(z) = -0.308 - 0.0724z - 0.0534z^2 + 0.0247z^3, \quad (2.13)$$

$$b_s(z) = -\frac{2}{7} [b_1(z) - 1]. \quad (2.14)$$

Here b_1, b_2 are cubic fits to halo model predictions, while b_s is the simplest tidal bias model, corresponding to vanishing initial tidal bias.

Figure 1 displays the lensing contribution to the reduced bispectrum in the equilateral configuration, colour-coded according to the multipole values ℓ , with all three redshifts the same (left) and with $z_1 = z_2 = 0.6$ and varying z_3 (right). The left panel shows that the lensing contribution in the equal-redshift case decreases as z and ℓ increase. The right panel shows that for two equal redshifts, the signal is greater when the third redshift is smaller – i.e., when the equal-redshift fluctuations are lensed by the lower redshift fluctuation. This is consistent with examples for galaxy surveys given in [6].

Figure 2 compares the lensing contribution to the unlensed reduced bispectrum in the equilateral configuration for various redshift triples. Appropriate smoothing of the unlensed bispectrum with a 15-point average filter has been performed where necessary (see [7, 13] for

¹<https://gitlab.com/montanari/byspectrum>

discussion of numerical issues in the redshift-space angular bispectrum). The bottom panels show a striking example of how the relative lensing contribution peaks when equal-redshift fluctuations are lensed by a lower redshift fluctuation. With high equal redshifts ($z \sim 3$), the lensing contribution can become comparable to, or even dominate over, the density and RSD contributions.

In Figure 3, the lensing contribution in isosceles configurations, $\ell_2 = \ell_3 \equiv \ell$ with $\ell_1 = 4$, is illustrated for the same redshift triples as the bottom row of Figure 2. For $\ell \gg 4$, we approach the squeezed limit. This case shows a similar behaviour to the equilateral, although the relative lensing contribution is higher in the equilateral case.

3 Discussion and conclusion

We derived the lensing contribution to the full-sky HI intensity mapping bispectrum in redshift space, at tree level, as given in (2.11). This generalises earlier results to include all RSD effects, as well as the clustering bias up to second order (including tidal bias). We presented some numerical examples for the equilateral configuration in Figures 1 and 2, and for the isosceles (including squeezed) configuration in Figure 3.

These examples suggest that the lensing contribution is greatest when two equal-redshift fluctuations are lensed by a lower redshift fluctuation, as expected from previous work on the galaxy bispectrum. For example, in the equilateral case with $z_1 = z_2 = 3$, $z_3 = 0.5$, the lensing contribution dominates in amplitude over the density and RSD contributions for $\ell \gtrsim 100$.

For other redshift configurations, including three equal redshifts, the lensing contribution is orders of magnitude below the unlensed contribution. Equation (2.11), shows that the 21cm lensing arises from terms of the form $C_\ell^{\Delta\Delta} C_{\ell'}^{\Delta\phi}$. The lensing contribution is only in $C_{\ell'}^{\Delta\phi}$, and for equal redshifts $C_\ell^{\Delta\Delta} \gg C_{\ell'}^{\Delta\phi}$ (for equal redshifts $C_\ell^{\Delta\phi} > 0$). As a consequence, the lensing effect is swamped by the contributions of density and RSD. A way out of this is if the redshifts are unequal, when it is possible (as shown in our examples) that the contribution of $C_\ell^{\Delta\Delta}$ is heavily suppressed while the lensing deflection can lead to an enhanced $C_{\ell'}^{\Delta\phi}$.

The relative 21cm lensing effect is typically much smaller than in galaxy surveys, for two reasons.

- There is a first-order lensing contribution for galaxies, proportional to the lensing convergence $\kappa^{(1)}$ [3], which is absent from 21cm intensity.
- At second order, the lensing effect in the 21cm bispectrum is from a single contribution, $L^{(2)} = \nabla_\perp^a \phi^{(1)} \nabla_{\perp a} \Delta^{(1)}$, whereas for galaxies, there are many more contributions, from $\kappa^{(2)}$, $[\kappa^{(1)}]^2$, $\kappa^{(1)} \Delta^{(1)}$, $\nabla_\perp^a \kappa^{(1)} \nabla_{\perp a} \phi^{(1)}$ (see [6]). It follows that the lensing effect for galaxies has pure-lensing and lensing \times (density + RSD) contributions, whereas for 21cm intensity, we have only a single lensing \times (density + RSD) contribution.

In our numerical examples we have used infinitely thin redshift bins. In the case of the galaxy angular power spectrum, it is known that increasing the width of redshift bins suppresses the density and RSD signals, but can increase the lensing contribution [14–16]. Similar behaviour is seen in the galaxy angular bispectrum [6]. By contrast, in the 21cm bispectrum the lensing contribution is typically *suppressed* by increasing the bin width.

The reason for this is again rooted in the fact that 21cm lensing is sourced by terms of the form $C_\ell^{\Delta\Delta} C_{\ell'}^{\Delta\phi}$. Although the cross-power spectrum with lensing, $C_{\ell'}^{\Delta\phi}$, may be enhanced

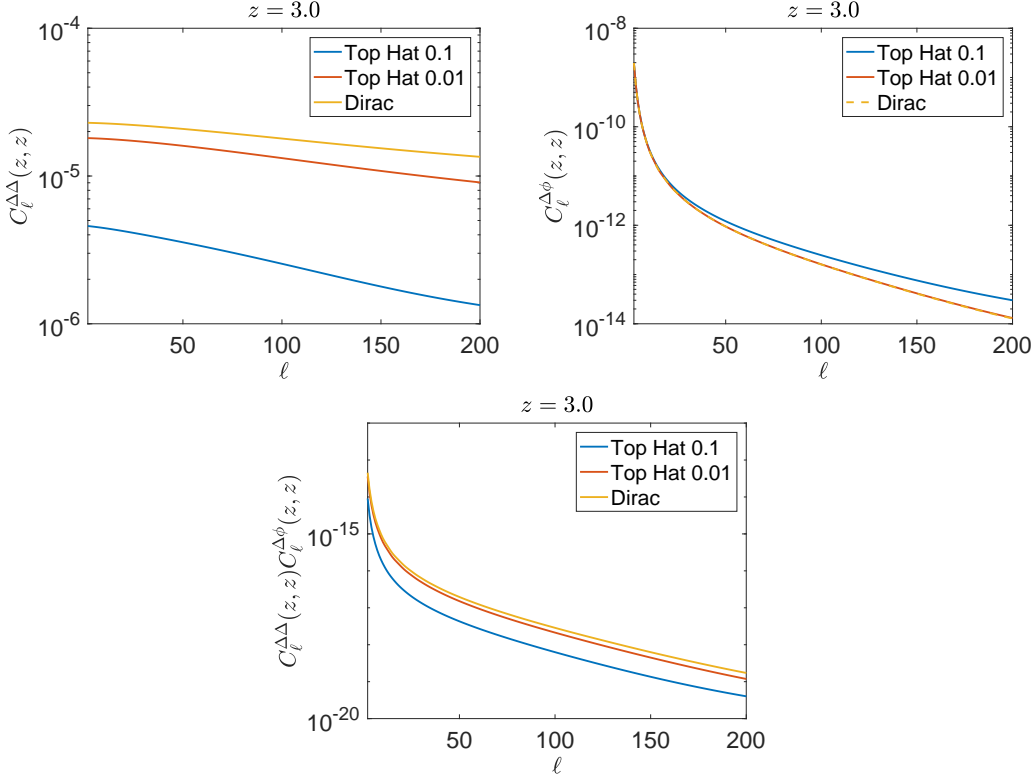


Figure 4. Effect of varying the z -bin width, using a top-hat window function, for an equilateral configuration and equal redshifts. *Top:* The 2 angular power spectra in the lensing reduced bispectrum (3.1). *Bottom:* The product of the power spectra.

by increasing the bin width, it is always multiplied by a non-lensing auto-power spectrum $C_\ell^{\Delta\Delta}$, which is suppressed by increasing the bin width.

This is illustrated by using redshift bins of width $\delta z = 0$ (Dirac delta window), 0.1 and 0.01, with a top-hat window function. We compute two equilateral examples as follows.

$z_i = z = 3$: The reduced lensing bispectrum (2.11) is

$$\delta b_{\ell\ell\ell}(z, z, z) = 3\alpha_\ell C_\ell^{\Delta\Delta}(z, z) C_\ell^{\Delta\phi}(z, z), \quad (3.1)$$

$$\alpha_\ell \equiv -2\ell(\ell+1) \begin{pmatrix} \ell & \ell & \ell \\ 0 & 0 & 0 \end{pmatrix}^{-1} \begin{pmatrix} \ell & \ell & \ell \\ 1 & -1 & 0 \end{pmatrix}. \quad (3.2)$$

Figure 4 shows the 2 power spectra in (3.1) (top panels) and then their product (bottom panel), which is proportional to the lensing contribution to the bispectrum. It can be seen that although the cross-power spectrum of lensing with HI intensity increases with bin width (top right panel), this contribution is overpowered by the effect of the HI auto-power spectrum, which decreases with bin width (top left). The lensing contribution to the bispectrum thus decreases with bin width, as follows from the bottom panel and (3.1).

$z_1 = z_2 \equiv z = 3, z_3 \equiv z' = 0.5$: The reduced lensing bispectrum (2.11) is

$$\delta b_{\ell\ell\ell}(z, z, z') = \alpha_\ell \mathcal{C}_\ell(z, z'), \quad (3.3)$$

$$\mathcal{C}_\ell(z, z') \equiv C_\ell^{\Delta\Delta}(z, z') C_\ell^{\Delta\phi}(z, z') + C_\ell^{\Delta\Delta}(z', z) C_\ell^{\Delta\phi}(z, z) + C_\ell^{\Delta\Delta}(z, z) C_\ell^{\Delta\phi}(z', z). \quad (3.4)$$

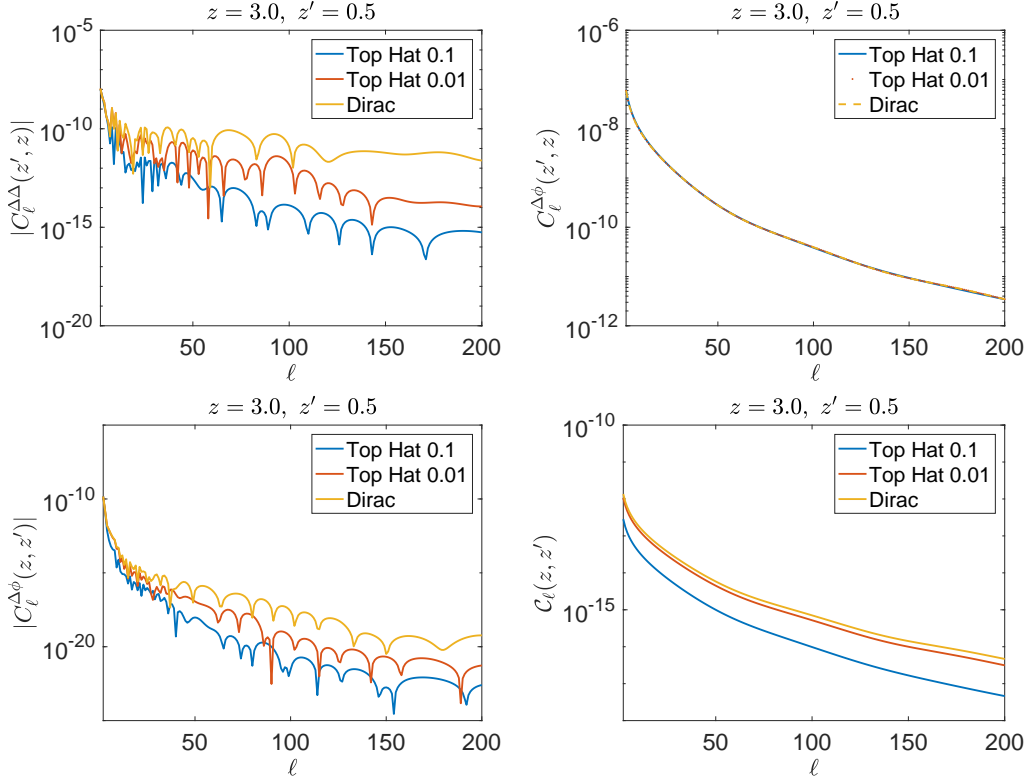


Figure 5. As in Figure 4, but with $z_1 = z_2 \equiv z = 3, z_3 \equiv z' = 0.5$. The angular power spectra in the lensing reduced bispectrum (3.4), in addition to the 2 in Figure 4, are shown in the top and bottom left panels. The bottom right panel shows \mathcal{C}_ℓ , defined in (3.4).

In this case, the two angular power spectra of (3.1) are included in (3.4), together with three further power spectra, noting that $C_\ell^{\Delta\Delta}(z', z) = C_\ell^{\Delta\Delta}(z, z')$. These three additional power spectra appearing in (3.4) are shown in Figure 5 (top panels and bottom left panel). The bottom left panel shows an example of a lensing contribution that decreases with bin width. Once again the total lensing contribution decreases with bin width, as follows from the bottom right panel and (3.4).

We have only considered a single redshift triple in our examples. In practice, the correlations from many triples will be added and this may enhance the lensing contribution. The 21cm bispectrum has been shown to be detectable by SKA (Phase 1) and HIRAX in [7], and therefore it could be measured using standard estimators in the literature. Detectability of the lensing contribution requires significant further work. Our initial rough estimates indicate that the signal to noise ratio of the lensing signal in equal-redshift bins for SKA1 and HIRAX is small and cross-bin correlations will need to be included for the possibility of a future detection.

Acknowledgements: We thank Ruth Durrer, Mona Jalilvand and Francesco Montanari for helpful comments, especially on Appendix B. RK thanks Saurabh Kumar for help with coding. RK and RM are supported by the South African Radio Astronomy Observatory and the National Research Foundation (Grant No. 75415). RM is also supported by the UK Science & Technology Facilities Council (Grant ST/S000550/1). This work made use of the South African Centre for High Performance Computing, under the project *Cosmology with Radio Telescopes*, ASTRO-0945.

A Derivation of (2.6)

The scalar product of screen-space derivatives of two spherical harmonics, which is needed to obtain the lensing contribution to the bispectrum in (2.6), can be written in terms of lowering and raising operators as [6]

$$\nabla_{\perp}^a Y_{\ell_3 m_3}(\mathbf{n}) \nabla_{\perp a} Y_{\ell_4 m_4}(\mathbf{n}) = \frac{1}{2} \left[\partial^* Y_{\ell_3 m_3}(\mathbf{n}) \partial Y_{\ell_4 m_4}(\mathbf{n}) + \partial Y_{\ell_3 m_3}(\mathbf{n}) \partial^* Y_{\ell_4 m_4}(\mathbf{n}) \right]. \quad (\text{A.1})$$

The effect of raising and lower operators on spherical harmonics is

$$\partial Y_{\ell m} = \sqrt{\ell(\ell+1)} {}_1 Y_{\ell m} \quad (\text{A.2})$$

$$\partial^* Y_{\ell m} = -\sqrt{\ell(\ell+1)} {}_{-1} Y_{\ell m}, \quad (\text{A.3})$$

where ${}_s Y_{\ell m}$ are spin-weighted spherical harmonics, which obey the product rule

$${}_s Y_{\ell_1 m_1} {}_s Y_{\ell_2 m_2} = \sum_{s \ell m} {}_s Y_{\ell m}^* \sqrt{\frac{(2\ell_1+1)(2\ell_2+1)(2\ell+1)}{4\pi}} \begin{pmatrix} \ell_1 & \ell_2 & \ell \\ m_1 & m_2 & m \end{pmatrix} \begin{pmatrix} \ell_1 & \ell_2 & \ell \\ -s_1 & -s_2 & -s \end{pmatrix}. \quad (\text{A.4})$$

Using (A.2) – (A.4), and symmetry properties of the Wigner 3j symbol, we obtain (2.6).

B Lensing correction to the tree-level 4-point correlation function

We denote by $\mathcal{O}(n)$ a perturbation of order n . Assuming that $\mathcal{O}(1)$ perturbations are Gaussian, the HI intensity mapping 4-point correlation function at tree level is $\langle \mathcal{O}(6) \rangle$, i.e., $\langle \mathcal{O}(1)\mathcal{O}(1)\mathcal{O}(2)\mathcal{O}(2) \rangle$ and $\langle \mathcal{O}(1)\mathcal{O}(1)\mathcal{O}(1)\mathcal{O}(3) \rangle$. We need to expand the lensed HI fluctuations to fourth order:

$$\begin{aligned} \Delta^L(z, \mathbf{n}) &= \Delta(z, \mathbf{n} + \nabla_{\perp} \phi(z, \mathbf{n})) \\ &= \Delta(z, \mathbf{n}) + \sum_{m=1}^4 \frac{1}{m!} \left[\nabla_{\perp}^{a_1} \phi \cdots \nabla_{\perp}^{a_m} \phi \nabla_{\perp a_1} \cdots \nabla_{\perp a_m} \Delta \right](z, \mathbf{n}) - \text{average} \\ &= \Delta(z, \mathbf{n}) + \sum_{m=1}^4 L^{(m)}(z, \mathbf{n}) - \langle L^{(2)} \rangle(z) - \langle L^{(4)} \rangle(z), \end{aligned} \quad (\text{B.1})$$

where all orders of ϕ and Δ that add to 4 or less are included in the sum and we assume that the average of Δ has been removed.

The lensing contribution to the 4-point correlation function only requires $L^{(2)}$ and $L^{(3)}$, and for these we need the lensing potential up to second order. At first order the lensing

potential is given by (1.2). At second order,

$$\phi^{(2)}(z, \mathbf{n}) = -2 \int_0^r dr_1 \frac{r - r_1}{rr_1} \varphi^{(2)}(z_1, \mathbf{n}) - 2 \int_0^r dr_1 \frac{r - r_1}{rr_1} \nabla_{\perp}^a \phi^{(1)}(z_1, \mathbf{n}) \nabla_{\perp a} \varphi^{(1)}(z_1, \mathbf{n}), \quad (\text{B.2})$$

where $\varphi = (\Phi + \Psi)/2$ and $r_i \equiv r(z_i)$. Here the terms which include $\nabla_{\perp}^a \varphi$ are the so-called post-Born terms, since they take into account the fact that the photon is not propagating along the unperturbed direction \mathbf{n} . With these expressions, the lensing correction to Δ at third order is

$$L^{(3)} = \nabla_{\perp}^a \phi^{(1)} \nabla_{\perp a} \Delta^{(2)} + \frac{1}{2} \nabla_{\perp}^a \phi^{(1)} \nabla_{\perp}^b \phi^{(1)} \nabla_{\perp a} \nabla_{\perp b} \Delta^{(1)} + \nabla_{\perp}^a \phi^{(2)} \nabla_{\perp a} \Delta^{(1)}, \quad (\text{B.3})$$

In a Λ CDM cosmology at late times, the Weyl potential and the metric potentials are equal at first order: $\varphi^{(1)} = \Phi^{(1)} = \Psi^{(1)}$. This also holds at higher order on sub-Hubble scales. Furthermore, the screen-space Laplacian of φ is well approximated by the 3D Laplacian on sub-Hubble scales and the Poisson equation maintains its Newtonian form. This implies that

$$\nabla_{\perp}^2 \varphi^{(n)} \simeq \nabla^2 \varphi^{(n)} \simeq \nabla^2 \Phi^{(n)} \simeq \frac{3}{2} \Omega_m \mathcal{H}^2 \delta^{(n)} \quad (\text{B.4})$$

where $\Omega_m \mathcal{H}^2 = \Omega_{m0} H_0^2 / a$ and $\delta^{(n)}$ is the Newtonian density contrast [17]. The lensed 4-point correlation function in redshift space is written as

$$T^L(z_i, \mathbf{n}_i) = \langle \Delta_1^L \Delta_2^L \Delta_3^L \Delta_4^L \rangle + \delta T(z_i, \mathbf{n}_i). \quad (\text{B.5})$$

Here δT is the lensing correction to the unlensed T . At tree level, the 4-point correlation function is of the form $\langle O(1)O(1)O(1)O(3) \rangle + \langle O(1)O(1)O(2)O(2) \rangle$. In detail

$$\begin{aligned} T^L(z_i, \mathbf{n}_i) &= \langle \Delta_1^{(1)} \Delta_2^{(1)} \Delta_3^{(1)} [\Delta_4^{(3)} + L_4^{(3)}] \rangle + 3 \text{ perms} \\ &+ \langle \Delta_1^{(1)} \Delta_2^{(1)} [\Delta_3^{(2)} + L_3^{(2)} - \langle L_3^{(2)} \rangle] [\Delta_4^{(2)} + L_4^{(2)} - \langle L_4^{(2)} \rangle] \rangle + 5 \text{ perms.} \end{aligned} \quad (\text{B.6})$$

The tree-level lensing correction is thus made up of two parts:

$$\delta T[1](z_i, \mathbf{n}_i) = \langle \Delta_1^{(1)} \Delta_2^{(1)} \Delta_3^{(1)} L_4^{(3)} \rangle + 3 \text{ perms}, \quad (\text{B.7})$$

$$\begin{aligned} \delta T[2](z_i, \mathbf{n}_i) &= \langle \Delta_1^{(1)} \Delta_2^{(1)} \Delta_3^{(2)} L_4^{(2)} \rangle - \langle \Delta_1^{(1)} \Delta_2^{(1)} \Delta_3^{(2)} \rangle \langle L_4^{(2)} \rangle + \langle \Delta_1^{(1)} \Delta_2^{(1)} \rangle \langle L_3^{(2)} \rangle \langle L_4^{(2)} \rangle \\ &+ \langle \Delta_1^{(1)} \Delta_2^{(1)} L_3^{(2)} \Delta_4^{(2)} \rangle + \langle \Delta_1^{(1)} \Delta_2^{(1)} L_3^{(2)} L_4^{(2)} \rangle - \langle \Delta_1^{(1)} \Delta_2^{(1)} L_3^{(2)} \rangle \langle L_4^{(2)} \rangle \\ &- \langle \Delta_1^{(1)} \Delta_2^{(1)} \Delta_4^{(2)} \rangle \langle L_3^{(2)} \rangle - \langle \Delta_1^{(1)} \Delta_2^{(1)} L_4^{(2)} \rangle \langle L_3^{(2)} \rangle + 5 \text{ perms.} \end{aligned} \quad (\text{B.8})$$

First consider $\delta T[1]$, which is obtained by using (B.3) in (B.7):

$$\begin{aligned} \delta T[1](z_i, \mathbf{n}_i) &= \langle \Delta_1^{(1)} \Delta_2^{(1)} \Delta_3^{(1)} \nabla_{\perp}^a \phi_4^{(1)} \Delta_{\perp a} \Delta_4^{(2)} \rangle + \frac{1}{2} \langle \Delta_1^{(1)} \Delta_2^{(1)} \Delta_3^{(1)} \nabla_{\perp}^a \phi_4^{(1)} \nabla_{\perp}^b \phi_4^{(1)} \nabla_{\perp a} \nabla_{\perp b} \Delta_4^{(1)} \rangle \\ &+ \langle \Delta_1^{(1)} \Delta_2^{(1)} \Delta_3^{(1)} \nabla_{\perp}^a \phi_4^{(2)} \Delta_{\perp a} \Delta_4^{(1)} \rangle + 3 \text{ perms.} \end{aligned} \quad (\text{B.9})$$

The other terms can be similarly obtained.

References

- [1] PLANCK collaboration, *Planck 2018 results. VIII. Gravitational lensing*, *Astron. Astrophys.* **641** (2020) A8 [[1807.06210](#)].
- [2] A. Hall, C. Bonvin and A. Challinor, *Testing General Relativity with 21-cm intensity mapping*, *Phys. Rev. D* **87** (2013) 064026 [[1212.0728](#)].
- [3] D. Alonso, P. Bull, P. G. Ferreira, R. Maartens and M. Santos, *Ultra large-scale cosmology in next-generation experiments with single tracers*, *Astrophys. J.* **814** (2015) 145 [[1505.07596](#)].
- [4] O. Umeh, R. Maartens and M. Santos, *Nonlinear modulation of the HI power spectrum on ultra-large scales. I*, *JCAP* **03** (2016) 061 [[1509.03786](#)].
- [5] M. Jalilvand, E. Majerotto, R. Durrer and M. Kunz, *Intensity mapping of the 21 cm emission: lensing*, *JCAP* **01** (2019) 020 [[1807.01351](#)].
- [6] E. Di Dio, R. Durrer, G. Marozzi and F. Montanari, *The bispectrum of relativistic galaxy number counts*, *JCAP* **01** (2016) 016 [[1510.04202](#)].
- [7] R. Durrer, M. Jalilvand, R. Kothari, R. Maartens and F. Montanari, *Full-sky bispectrum in redshift space for 21cm intensity maps*, *JCAP* **12** (2020) 003 [[2008.02266](#)].
- [8] A. Lewis and A. Challinor, *Weak gravitational lensing of the CMB*, *Phys. Rept.* **429** (2006) 1 [[astro-ph/0601594](#)].
- [9] J. R. Pritchard and A. Loeb, *21-cm cosmology*, *Rept. Prog. Phys.* **75** (2012) 086901 [[1109.6012](#)].
- [10] H. T. Johansson and C. Forssén, *Fast and accurate evaluation of Wigner 3j, 6j, and 9j symbols using prime factorisation and multi-word integer arithmetic*, *SIAM J. Sci. Statist. Comput.* **38** (2016) A376 [[1504.08329](#)].
- [11] D. Blas, J. Lesgourgues and T. Tram, *The Cosmic Linear Anisotropy Solving System (CLASS) II: Approximation schemes*, *JCAP* **07** (2011) 034 [[1104.2933](#)].
- [12] J. Lesgourgues, *The Cosmic Linear Anisotropy Solving System (CLASS) I: Overview*, [1104.2932](#).
- [13] E. Di Dio, R. Durrer, R. Maartens, F. Montanari and O. Umeh, *The Full-Sky Angular Bispectrum in Redshift Space*, *JCAP* **04** (2019) 053 [[1812.09297](#)].
- [14] E. Di Dio, F. Montanari, R. Durrer and J. Lesgourgues, *Cosmological Parameter Estimation with Large Scale Structure Observations*, *JCAP* **01** (2014) 042 [[1308.6186](#)].
- [15] W. Cardona, R. Durrer, M. Kunz and F. Montanari, *Lensing convergence and the neutrino mass scale in galaxy redshift surveys*, *Phys. Rev. D* **94** (2016) 043007 [[1603.06481](#)].
- [16] G. Jelic-Cizmek, F. Lepori, C. Bonvin and R. Durrer, *On the importance of lensing for galaxy clustering in photometric and spectroscopic surveys*, [2004.12981](#).
- [17] F. Bernardeau, S. Colombi, E. Gaztanaga and R. Scoccimarro, *Large scale structure of the universe and cosmological perturbation theory*, *Phys. Rept.* **367** (2002) 1 [[astro-ph/0112551](#)].